

# IVIM analysis of brain tumors: an investigation of the relaxation effects of CSF, blood, and tumor tissue on the estimated perfusion fraction

Sotirios Bisdas · Uwe Klose

Received: 29 April 2014 / Revised: 16 November 2014 / Accepted: 21 November 2014 / Published online: 5 December 2014  
© ESMRMB 2014

## Abstract

**Object** We sought to investigate the dependence of intravoxel incoherent motion (IVIM)-related perfusion fraction ( $f$ ) estimates on the transverse relaxation of brain tissue, blood, and cerebrospinal fluid (CSF), attempting to overcome the influence of CSF on conventional  $f$  maps.

**Materials and methods** Eighteen patients with gliomas underwent DWI with 14 b-values (0–1,300 s/mm<sup>2</sup>) and two distinct echo times (TEs). Regions of interest representing tumour and normal brain tissue were analysed by calculating the  $f$  values for both TEs. A mask for pixels with relevant CSF partial volume was subsequently created. The  $f$  values were tested for significant differences.

**Results** We found statistically significant differences between the two TEs in the  $f$  values for cortical and juxtacortical structures and non-enhancing areas of the tumour/oedema. Normal white matter and gadolinium-enhancing tumour tissue appeared insensitive to TE variation. In all tissue types examined, the masking of voxels with considerable CSF content was able to overcome issues of erroneous  $f$  estimation and calculation of  $f$  values insensitive to TE changes was feasible.

**Conclusion** Due to the complex interaction in the relaxation rates of CSF, blood, and tumour tissue, the estimation of  $f$  values is affected by the choice of TE. Only  $f$  values in normal white matter and tumour tissue—which largely comprise blood voxels with minor CSF partial volume—may be clinically applicable in the present form of IVIM-based DWI analysis. Going a step further, and after removing voxels with heavily TE-susceptible  $f$  values, we were

able to obtain accurate and TE-independent  $f$  values in contrast-enhancing tumour tissue, white matter, and grey matter, which were essentially consistent with those reported in the literature.

**Keywords** DWI · IVIM · Perfusion · Brain tumour

## Introduction

According to intravoxel incoherent motion (IVIM)-based DWI analysis, the signal decay in normal brain tissue can be bi-exponentially fitted within the range of the applied b-values, and blood flow in capillaries may be the main contributing factor to non-mono-exponential decay in brain tissue [1]. The early reports on IVIM-based DWI analysis by Le Bihan et al. [1, 2] stressed the potential of the method to shed light in the area of molecular motion in neurological disorders. IVIM also demonstrated sensitivity in measuring changes in cerebral blood flow under suppression of extravascular water signals in an experimental setting in a rat brain [3]. Recently, the bi-exponential behavior of signal decay in brain tumours was demonstrated, and its clinical application may include tumour grading [4, 5] and differentiation of recurrent tumours from post-treatment effects [6].

The IVIM-modeled DWI of the brain, however, has two inherent shortcomings. Firstly, the cerebrospinal fluid (CSF) space may act as a third compartment, with similar diffusion-dependent signal decay to blood [2], and thus may contribute significantly to the measured perfusion in parts of the brain with considerable CSF partial volume. Secondly, the relaxation effects of blood and tissue are neglected in the IVIM model. We sought to determine the magnitude of perfusion fraction ( $f$ ) error in brain tissue and tumours due

S. Bisdas (✉) · U. Klose  
Department of Neuroradiology, Eberhard Karls University,  
Hoppe-Seyler-Str. 3, 72076 Tübingen, Germany  
e-mail: sotirios.bisdas@uni-tuebingen.de

to CSF and blood, as well as its dependence on echo time (TE). In this context, we performed DWI experiments with different TEs under the assumption that the different transverse relaxation times of normal-appearing white matter, grey matter, blood, and CSF [7] would have an influence on  $f$  values. Subsequently, we postulated that since the transverse relaxation time of blood and CSF is significantly different, the signal behavior from blood and CSF, measured as a function of b-values under varying echo times, would differ, and might allow segmentation of the CSF-filled spaces and extraction from conventional  $f$  maps.

## Materials and methods

Eighteen patients (7 women, 11 men; median age, 54 (range 42–71) years) with brain tumours underwent DWI as part of presurgical MR imaging workup prior to any therapy. The primary sites of the gliomas included the occipital lobe ( $n = 4$ ), frontal lobe ( $n = 8$ ), temporal lobe ( $n = 4$ ), and parietal lobe ( $n = 2$ ). The histological grading showed nine low-grade (WHO grade II) gliomas and nine high-grade (WHO grade III–IV) tumours.

Imaging was performed using a 3T MR scanner (MAGNETOM Verio; Siemens Healthcare, Erlangen, Germany), including axial T2-weighted FLAIR (repetition time in ms/echo time in ms, 9,000/103) MR images, and T1-weighted images (TR/TE: 450/15 ms), before and after intravenous administration of a body-weight-adapted dose of gadobutrol (Gadovist<sup>®</sup>, Bayer-Schering, Berlin, Germany), followed by a 20-ml saline flush. DWI was performed prior to any contrast agent administration, using two different TEs (TE<sub>1</sub>/TE<sub>2</sub>: 60/150 ms) based on standard single-shot DW spin-echo echo-planar imaging (EPI) using a monopolar Stejskal–Tanner implementation with the following parameters (which remained unchanged between the two acquisitions): TR 3,300 ms, GRAPPA acceleration factor 2, field of view 230 × 230, base resolution 128 × 128, 10 slices with thickness 3 mm, intersection gap 3 mm, number of averages 2, bandwidth 751 Hz,  $\delta = 26.5$  ms,  $\Delta = 39.9$  ms (TE = 60 ms), acquisition time of each DWI measurement 3 min 50 sec. The axial three-scan trace DW images were acquired with multiple b-values, ranging from 0 s/mm<sup>2</sup> to 1,300 s/mm<sup>2</sup> (0, 5, 10, 20, 30, 40, 60, 80, 90, 100, 200, 700, 1,000, 1,300). Adequate signal-to-noise ratio (SNR) was achieved in TE = 150 ms in all patients, and an illustrative example of the acquired DWI-source images with both TEs is given in Fig. 1.

### Post-processing of DW-MR imaging

The data collection and analysis was performed in a blind fashion. Image distortion was corrected online for

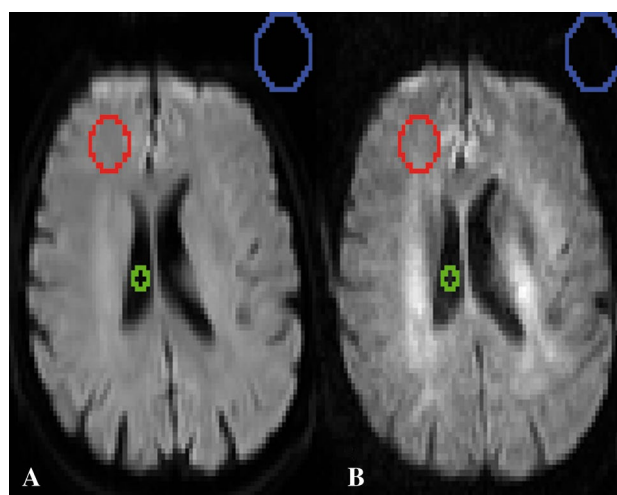
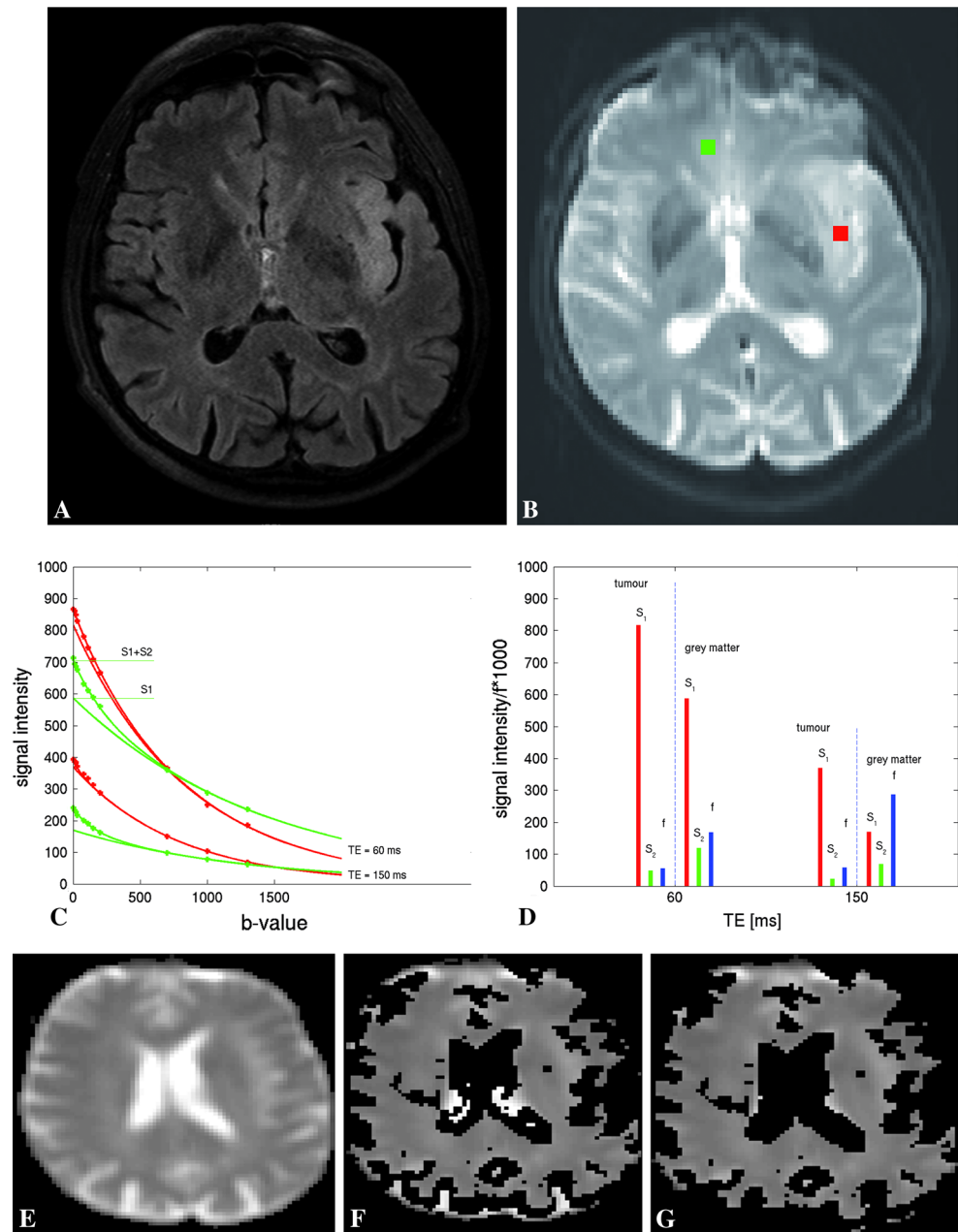


**Fig. 1** Illustrative example of a DWI-source slice measured with a b-value of 1,300 mm<sup>2</sup>/sec and echo times of 60 ms (a) and 150 ms (b). The signal intensities in the marked regions were: brain tissue (in red) 197.0 and 50.0, CSF (in green) 23.3 and 13.2, and background noise (in blue) 3.7 and 2.4, for TEs of 60 ms and 150 ms, respectively. The SNR in the long-TE and high-b-value images was approximately 20 for brain tissue and still >10 for CSF

all DWI images. In the  $b = 0$  s/mm<sup>2</sup> images obtained with TE<sub>1</sub> = 60 ms, 3–4 standardized regions of interest (ROIs) (3 × 3 pixels) were drawn in selected slices representing different tumour regions, including enhancing and non-enhancing areas (oedema or low-grade areas of the tumour), as well as normal brain tissue. The ROIs in  $b = 0$  s/mm<sup>2</sup> images were identical for both data sets. Evaluation of the decay of the mean signal in these ROIs was performed in a two-step procedure. In the first step, a mono-exponential function was fitted to the mean signal values of the group of higher b-values (700; 1,000; 1,300 s/mm<sup>2</sup>). The obtained fit-function with the apparent diffusion coefficient  $D$  and the extrapolated signal  $S_1$  at  $b = 0$  s/mm<sup>2</sup> was subtracted from the measured signal intensity curve, and a second mono-exponential fit-function was performed using all measured b-values, yielding the apparent diffusion coefficient  $D^*$  and signal intensity  $S_2$  at  $b = 0$  s/mm<sup>2</sup>. Apparent perfusion  $f$  values were calculated as  $f = S_2 / (S_1 + S_2)$  (Fig. 2). This evaluation was performed on both data sets measured at TE<sub>1</sub> = 60 ms and TE<sub>2</sub> = 150 ms.

Based on  $S_1$  and  $S_2$  values from both TEs, transversal relaxation time in the slow ( $T_{2\text{slow}}$ ) and fast ( $T_{2\text{fast}}$ ) diffusion phases was determined using a pixel-wise calculation (Fig. 2). Following our hypothesis,  $T_{2\text{slow}}$  and  $T_{2\text{fast}}$  may allow a determination of whether the selected ROI contains relevant partial volume of CSF. If the measured  $T_2$  value of the signal component  $S_2$  has a high value, the origin of this compartment can be assigned as CSF, and the apparent  $f$  can no longer be assigned to describe perfusion.

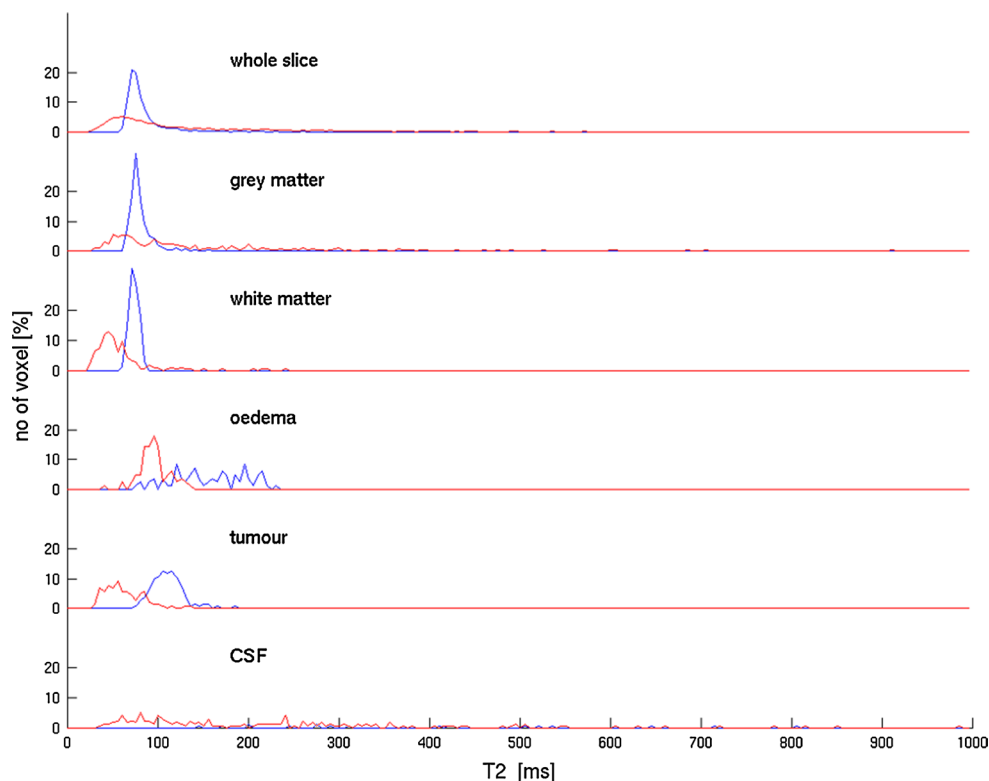
**Fig. 2** Schematic workflow of image post-processing in a patient with a WHO grade III glioma on the left temporal lobe, as demonstrated in the FLAIR image (a). For illustrative purposes, regions of interest (ROIs) encompassing tumour tissue (*red*) and (juxta)cortical normal structures (*green*) are drawn on the source DWI image ( $b = 0 \text{ s/mm}^2$ ) (b), and signal decay curves are plotted for echo times of both 60 ms and 150 ms (c). The  $f$  is estimated by the equation  $f = S_2/(S_1 + S_2)$  (see text in [Materials and Methods](#)). The effect of TE on  $f$  values is also schematically illustrated in (d), where a significant increase for the grey matter is seen on the longer TE. After pixel-wise calculation of the  $T2_{\text{slow}}$  and  $T2_{\text{fast}}$  maps at the level of the upper tumour border, as demonstrated in (e), an initial threshold ( $T2_{\text{fast}} > 100 \text{ ms}$ ) is applied to mask the voxels with relevant CSF contribution (f). The additional benefit from applying the  $T2_{\text{slow}} > 200 \text{ ms}$  condition is the further elimination of voxels with large CSF content, as shown in the ventricles as well as in the sulci in (g)



Theoretically, a mask for pixels with relevant CSF partial volume can be created, and pixels within this mask may be subsequently excluded from the ROI evaluation. The thresholds of the  $T2$  values for this mask may be arbitrarily defined if we consider the following approximations of  $T2$  values in brain tissues. The transverse relaxation time of the white and grey matter at  $3T$  is assumed to be 80 ms [7], while the transverse relaxation time in tumour tissue may be longer (up to 200 ms). The transverse relaxation time of blood at  $3T$  depends on the oxygenation level, and is in the range of 80–120 ms [8, 9], considering that the blood water  $T2$  value was reported to be approximately 127 and 163 ms at 1.5  $T$  for an oxygen fraction of 0.6 and 0.7, respectively

[10], and the  $T2$  also decreases with increasing  $B_0$  [11]. Finally, the transverse relaxation time of CSF should be much longer, and relevant CSF partial volume would increase the  $T2_{\text{fast}}$  value. Nonetheless, in the case of significant CSF partial volume, the CSF contributes to the signal component  $S_1$ , and it may be difficult to identify the fast-decaying signal component. Considering all of the aforementioned facts, two conditions—namely,  $T2_{\text{slow}} > 200 \text{ ms}$  and  $T2_{\text{fast}} > 100 \text{ ms}$ —were applied for pixel inclusion in the CSF mask. Figure 2 demonstrates an example of CSF mask as well as the advantage of combining two thresholds for  $T2_{\text{slow}}$  and  $T2_{\text{fast}}$ , rather than the single threshold for  $T2_{\text{fast}}$ . Figure 3 demonstrates illustratively the distinct

**Fig. 3** Voxel histograms (in %) showing the distribution of  $T2_{\text{slow}}$  and  $T2_{\text{fast}}$  values in different tissue types of a patient with WHO grade IV glioma. The blue lines depict the distribution of  $T2_{\text{slow}}$  values, whereas the red lines show the  $T2_{\text{fast}}$  distribution. Pixels with calculated  $T2$  values larger than 1,000 ms (e.g., in CSF) were also counted (data not shown)



histogram distribution of  $T2_{\text{slow}}$  and  $T2_{\text{fast}}$  values among the voxels in different types of tissue.

#### Statistical analysis

The  $f$  values obtained in selected regions with  $TE_1$  and  $TE_2$ , both before and after application of the CSF mask, were tested for significant differences using a paired-samples  $t$  test (MedCalc Statistical Software version 12.7.2, MedCalc Software bvba, Ostend, Belgium).  $P$  values  $< 0.05$  were considered statistically significant.

#### Results

All experiments resulted in diffusion-weighted images with adequate SNR ratios, subsequently resulting in post-processed  $f$  maps of sufficient quality. Figure 2 shows an illustrative case of a patient with a high-grade glioma, including ROI analysis, signal decay curves, and the effect of TE on  $f$  for grey matter and tumour tissue. Figure 3 demonstrates the histogram distribution of  $T2_{\text{slow}}$  and  $T2_{\text{fast}}$  values in the grey and white matter, enhancing tumour, and surrounding oedema in a patient with a WHO grade IV glioma. The extracted  $f$  values from the DWI measurements with both TEs are shown in Table 1. Table 2 shows the diffusivity of each tissue type with both TEs. In the grey matter ROIs, there was a clear difference

between the  $f$  values obtained with both echo times, indicating a considerable influence of CSF on the signal component  $S_2$ . On the other hand, in the gadolinium-enhancing tumour regions, the  $f$  values were non-significantly increased with longer TE, likely indicating less CSF contamination. After application of the CSF mask, the  $f$  maps showed no significant changes between  $f_{\text{original}}$  and  $f_{\text{mask}}$  for the white matter and tumour tissue, again indicating negligible and marginal CSF (or CSF-like) voxel contamination, respectively. The  $f_{\text{mask}}$  value in the grey matter was significantly lower than the  $f_{\text{original}}$  (mean difference: 0.04;  $P = 0.0002$ ). Interestingly, the suppression of CSF-contaminated voxels by the mask did not affect  $f$  maps in any other types of tissue.

#### Discussion

Notably, the original IVIM analysis ignores all relaxation effects. In brain imaging at  $3T$ , white and grey matter have demonstrated region-dependent  $T2$  values of 70–80 and 100–130 ms, respectively [7, 12]. Other authors conducting similar measurements after segmentation of white and grey matter found  $T2$  values of approximately 90 ms for both tissue types [13]. Prolonged  $T2$  relaxation time in tissue can be seen in tumours ( $T2$  values of approximately 180 ms in enhancing and non-enhancing tumour areas and approximately 210 ms in surrounding oedema

**Table 1** Descriptive statistics of the calculated  $f$  values of normal gray and white matter, and contrast-agent-enhancing and non-enhancing tumour/oedema tissue in 18 patients

	Grey matter	White matter	Contrast-enhancing tumour	Non-enhancing tumour/oedema
TE = 60 ms (without CSF mask)	0.15 ± 0.03*	0.12 ± 0.02	0.15 ± 0.04 <sup>†</sup>	0.15 ± 0.02
TE = 150 ms (without CSF mask)	0.25 ± 0.08**	0.14 ± 0.02	0.18 ± 0.09 <sup>‡</sup>	0.12 ± 0.03
<i>P</i> value	<b><i>P</i> &lt; 0.001</b>	<i>P</i> = 0.06	<i>P</i> = 0.08	<b><i>P</i> = 0.05</b>
TE = 60 ms (with CSF mask)	0.12 ± 0.01*	0.12 ± 0.02	0.12 ± 0.02 <sup>†</sup>	0.15 ± 0.06
TE = 150 ms (with CSF mask)	0.12 ± 0.02**	0.13 ± 0.02	0.13 ± 0.04 <sup>‡</sup>	0.13 ± 0.02
<i>P</i> value	<i>P</i> = 0.34	<i>P</i> = 0.06	<i>P</i> = 0.23	<i>P</i> = 0.08

The *P* values (significant values indicated in **bold**) of the respective comparisons between  $f$  values from both TEs without (*upper three rows*) and with (*lower three rows*) suppression of CSF-containing voxels are also demonstrated. Any significant (or tendencies to significance) different  $f$  values in each tissue type after applying the mask are indicated with *asterisks* or *daggers*

\*  $P = 0.0002$ , \*\*  $P < 0.0001$ , <sup>†</sup>  $P = 0.054$ , <sup>‡</sup>  $P = 0.01$

**Table 2** Slow ( $D$ ) and fast ( $D^*$ ) diffusivity values (in  $10^{-3}$  mm<sup>2</sup>/s) of each tissue type for both TEs used, with no compensation for CSF-containing voxels

	$D$		$D^*$	
	TE = 60 ms	TE = 150 ms	TE = 60 ms	TE = 150 ms
Grey matter	0.67	0.70	4.85	5.02
White matter	0.62	0.61	3.74	3.75
Contrast-enhancing tumour tissue	0.86	0.87	4.44	4.44
Non-enhancing tumour/oedema	0.94	0.95	4.59	4.56

[14, 15]) and in brain tissue post-treatment regimens, where high  $T_2$  is also a frequent side effect of radio- and/or chemotherapy as well as of radiation injury [16]. A difference in  $T_2$  times between blood and tissue will inevitably influence the ratio between the signal components  $S_1$  and  $S_2$ , and therefore will affect the calculated  $f$  value. In this context, Lemke et al. examined the effect of TE on  $f$  values in tissues with significantly shorter  $T_2$  times (e.g., in the pancreas). They reported a positive correlation between increasing TE and  $f$  in pancreatic tissue, and thus proposed a modification of the IVIM equation incorporating the effects of relaxation [17]. The relaxation-time-compensated value of  $f$  was then almost identical at all TEs. Based on the modified IVIM equation [17], Hales and Clark implemented an inversion pulse at the start of the brain DWI sequence for CSF suppression and accounted for it in the calculation of TE-insensitive IVIM parameters in healthy subjects [18].

In our study, the  $f$  values in the three types of brain tissue—namely, grey matter, white matter, and tumour tissue—demonstrated distinct behaviour during the two TE measurements, indicating the need to consider relaxation effects in IVIM imaging. In contrast, the diffusivity values, as shown in Table 1, were unaffected by the difference in TEs, in accordance with results achieved by Lemke et al. [17]. Compared to previous studies [17, 18], our measurements accounted not only for healthy tissue with shorter  $T_2$  than blood water (e.g., grey and white matter), but also for

pathologic structures with higher  $T_2$  values (e.g. tumours/oedema), as well as for the CSF compartment, which is a distinguishing feature and at the same time a drawback in brain IVIM-based analysis. The  $f$  values in grey matter were significantly affected by contamination with CSF. This was evidenced by the elevation of  $f$  values in measurements with higher TEs in the cortical and juxtacortical structures, as well as the fact that the non-CSF-compensated grey matter  $f$  values were markedly higher than the tumour  $f$  values (TE = 150 ms). The reason for this is the higher  $T_2$  of the CSF compared to the other tissue types, which leads to an increased  $S_2$  fraction, and subsequently to an overestimation of  $f$  with higher TEs; this phenomenon is illustrated in Fig. 2d.

The  $f$  values in tumour tissues in our patient cohort were consistent with those in previously published studies [4, 5]. The non-significant increase in the  $f$  values of gadolinium-enhancing tumour tissue with increasing TEs may be attributable to the marginal CSF contamination in tumour tissue, presumably that arising from grey matter, as well as to the high  $T_2$  relaxation time in certain areas of the tumour environment (compare also to Fig. 3 concerning the distribution of  $T_2$  in tumor tissue). The first assumption is borne out by the lower  $f$  values in contrast-enhancing tumour areas after CSF artefact compensation. The significant susceptibility of the  $f$  values in the surrounding tumour oedema (or non-enhanced tumour) on TE—namely, the decrease in  $f$  values with increasing TE—is due to the increased  $T_2$  of



this tissue type compared to blood and enhancing tumour tissue. This leads to an increase in  $S1$  at a TE of 160 ms, and thus to a higher denominator in the  $f$  equation, resulting in lower values of  $f$  with higher TEs, an effect that persisted even after the CSF mask was applied. In other words, as the TE increases, we expect that the signal contribution of oedematous tissue becomes more dominant relative to the blood compartment [19], inevitably leading to a further decrease in  $f$  values.

The  $f$  values in white matter did not undergo any significant change with increasing TE, which may be explained in consideration of a lower (or negligible) CSF fraction compared to cortical structures [20] and an insufficient difference in  $T2$  values between blood and white matter. In our work, blood was assumed to predominantly represent the arterial (or normoxic) fraction, which is significantly more attenuated by diffusion gradients as a result of its pulsatile and more turbulent nature compared to the venous (less oxygenated) fraction [21]. The extent to which IVIM gradients can suppress an intravenous signal is dependent on vessel size, and remains controversial [22]. Our finding is generally discordant with previous experience, where after applying an inversion recovery sequence an attenuation (about 4 %) of the fast component was observed in white matter regions even those that were chosen to avoid CSF partial volume effect as best as possible [23]. Interestingly, Falconer and Narayana observed an affect on ADC values after CSF suppression even in regions that were relatively remote from CSF, which they attributed to partial volume averaging. In their case, we assume that the result may be due to partial flow compensation of blood in tissue after the IR pulse [24, 25].

Although our patient sample was limited, our experimental findings shed light on the TE-dependent nature of IVIM-based estimation of  $f$  values in regions of normal brain tissue and brain tumours. Moreover, the results have important clinical implications, since IVIM has been proposed for discriminating between low- and high-grade tumours as well as between tumour recurrence and post-therapeutic tissue injury [4–6]. Indeed, cortical or juxtacortical structures that may have relevant CSF partial volume cannot serve as reference tissue, whereas any longitudinal  $f$  measurements in the vicinity of these structures should strictly follow identical experimental conditions with respect to the TE. The  $f$  measurements in tumours that are primarily located adjacent to the brain cortex may be artificially high, and estimations of  $f$  values in patients with pronounced oedema may not be reproducible across institutions. Solutions to this methodological drawback, therefore, are needed in order to exploit the potential of IVIM analysis. In this context, DWI schemes with two or more echoes extrapolating to TE = 0 or simultaneously incorporating relaxation effects in the calculation of a relaxation-compensated  $f$  [17], while computationally complex, could

be interesting approaches for validation of initial clinical results [4–6], and may be useful for the clinical dissemination of this methodology.

On the other hand, our approach to this problem by masking the CSF effect proved to be feasible and robust. The “CSF fraction”-compensated  $f$  calculations in cortical/juxtacortical and enhancing tumour tissue were significantly lower than the original estimates in both TEs ( $P \leq 0.0002$ ), and interestingly, proved to be immune to any variability in TE. The compensated  $f$  values were higher than those experimentally reported by Le Bihan in a study of the cerebral cortex of a cat [26], and were lower than those found by Hales and Clark, who examined healthy young subjects—mean age, 27 years—using a TE of 120 ms at  $1.5T$  after implementation of a CSF-suppressed inversion recovery (IR) pulse sequence [18]. The potential clinical attractiveness of the masked  $f$  maps compared to other methods employing IR pulse sequences for eliminating CSF flow-related artefacts is its relative simplicity [27]. CSF-suppressed DWI may fail to completely rule out the contaminating CSF signal, given the high diffusion constant of CSF and its non-laminar flow, which may have unpredictable effects on signal attenuation by IR DWI in the ventricles as well as in the sulcal interface [28, 29]. CSF-sensitized sequences demand higher TE values during the acquisition as well as increased bandwidth to account for adequate suppression of the inflow phenomenon. Moreover, they are vulnerable to eddy currents and motion artefacts (multi-shot EPI sequences in particular), which may, in turn, increase with the gradient strength used. An inversion pulse applied at the start of a DWI sequence may also result in differences in longitudinal magnetization relaxation times of blood and tissue (the magnitude of the attenuation may reach 30 %), which must then be accounted for in the post-processing, and likely result in reduced  $f$  values [23]. Furthermore, it has been demonstrated that the optimal inversion time (TI) is dependent on the region of the brain (e.g., cortical regions are better CSF-suppressed than ventricle regions with shorter TI), but at the same time must be sufficiently long to allow measurement of fresh inflowing blood with fully relaxed longitudinal magnetization at  $t = TI$ , resulting in an imperfect tradeoff for whole-brain CSF suppression [29].

## Conclusion

In the present work, we confirmed our hypothesis regarding the dependence of IVIM-based calculation of  $f$  values on TE for normal brain tissue and brain tumours due to the complex interaction among CSF, blood, and tumour tissue. The  $f$  values were fairly constant on gadolinium-enhancing tumour tissue, whereas they showed large variation in

cortical and juxtacortical voxels, chiefly representing grey matter voxels, and to a smaller extent in non-enhancing tumour/oedematous tissue. Based on our proposed method for masking voxels with pronounced TE susceptibility, accurate and echo-time-independent  $f$  values were obtained in all tissue types, including contrast-enhancing tumour tissue, grey and white matter.

**Conflict of interest** The authors each declare that they have no conflict of interest.

**Ethical standards** All human and animal studies were approved by the appropriate ethics committee and were therefore performed in accordance with the ethical standards laid down in the 1964 Declaration of Helsinki and its later amendments. All persons gave their informed consent in written form prior to their inclusion in the study. Details that might disclose the identity of the subjects under study were omitted.

## References

1. Le Bihan D, Breton E, Lallemand D, Aubin ML, Vignaud J, Laval-Jeantet M (1988) Separation of diffusion and perfusion in intravoxel incoherent motion MR imaging. *Radiology* 168(2):497–505
2. Le Bihan D, Breton E, Lallemand D, Grenier P, Cabanis E, Laval-Jeantet M (1986) MR imaging of intravoxel incoherent motions: application to diffusion and perfusion in neurologic disorders. *Radiology* 161(2):401–407
3. Neil JJ, Bosch CS, Ackerman JJ (1994) An evaluation of the sensitivity of the intravoxel incoherent motion (IVIM) method of blood flow measurement to changes in cerebral blood flow. *Magn Reson Med* 32(1):60–65
4. Bisdas S, Koh TS, Roder C, Braun C, Schittenhelm J, Ernemann U, Klose U (2013) Intravoxel incoherent motion diffusion-weighted MR imaging of gliomas: feasibility of the method and initial results. *Neuroradiology* 55(10):1189–1196
5. Federau C, Meuli R, O'Brien K, Maeder P, Hagmann P (2014) Perfusion measurement in brain gliomas with intravoxel incoherent motion MRI. *AJNR Am J Neuroradiol* 35(2):256–262
6. Kim HS, Suh CH, Kim N, Choi CG, Kim SJ (2014) Histogram analysis of intravoxel incoherent motion for differentiating recurrent tumor from treatment effect in patients with glioblastoma: initial clinical experience. *AJNR Am J Neuroradiol* 35(3):490–497
7. Stanisz GJ, Odobina EE, Pun J, Escaravage M, Graham SJ, Bronskill MJ, Henkelman RM (2005) T1, T2 relaxation and magnetization transfer in tissue at 3T. *Magn Reson Med* 54(3):507–512
8. Meyer ME, Yu O, Eclancher B, Grucker D, Chambron J (1995) NMR relaxation rates and blood oxygenation level. *Magn Reson Med* 34(2):234–241
9. Silvennoinen MJ, Clingman CS, Golay X, Kauppinen RA, van Zijl PC (2003) Comparison of the dependence of blood R2 and R2\* on oxygen saturation at 1.5 and 4.7 Tesla. *Magn Reson Med* 49(1):47–60
10. Wright GA, Hu BS, Macovski A (1991) Estimating oxygen saturation of blood in vivo with MR imaging at 1.5 T. *J Magn Reson Imaging* 1(3):275–283
11. Lin AL, Qin Q, Zhao X, Duong TQ (2012) Blood longitudinal (T1) and transverse (T2) relaxation time constants at 11.7 Tesla. *Magn Reson Mater Phy* 25(3):245–249
12. Wansapura JP, Holland SK, Dunn RS, Ball WS Jr (1999) NMR relaxation times in the human brain at 3.0 tesla. *J Magn Reson Imaging* 9(4):531–538
13. Oros-Peusquens AM, Laurila M, Shah NJ (2008) Magnetic field dependence of the distribution of NMR relaxation times in the living human brain. *Magn Reson Mater Phy* 21(1–2): 131–147
14. Hattingen E, Jurcoane A, Daneshvar K, Pilatus U, Mittelbronn M, Steinbach JP, Bahr O (2013) Quantitative T2 mapping of recurrent glioblastoma under bevacizumab improves monitoring for non-enhancing tumor progression and predicts overall survival. *Neuro Oncol* 15(10):1395–1404
15. Oh J, Cha S, Aiken AH, Han ET, Crane JC, Stainsby JA, Wright GA, Dillon WP, Nelson SJ (2005) Quantitative apparent diffusion coefficients and T2 relaxation times in characterizing contrast enhancing brain tumors and regions of peritumoral edema. *J Magn Reson Imaging* 21(6):701–708
16. Miot-Noirault E, Akoka S, Hoffschir D, Pontvert D, Gaboriau G, Alapetite C, Fetissou F, Le Pape A (1996) Potential of T2 relaxation time measurements for early detection of radiation injury to the brain: experimental study in pigs. *AJNR Am J Neuroradiol* 17(5):907–912
17. Lemke A, Laun FB, Simon D, Stieltjes B, Schad LR (2010) An in vivo verification of the intravoxel incoherent motion effect in diffusion-weighted imaging of the abdomen. *Magn Reson Med* 64(6):1580–1585
18. Hales PW, Clark CA (2013) Combined arterial spin labeling and diffusion-weighted imaging for noninvasive estimation of capillary volume fraction and permeability-surface product in the human brain. *J Cereb Blood Flow Metab* 33(1):67–75
19. Chien D, Levin DL, Anderson CM (1994) MR gradient echo imaging of intravascular blood oxygenation: T2\* determination in the presence of flow. *Magn Reson Med* 32(4):540–545
20. Piechnik SK, Evans J, Bary LH, Wise RG, Jezzard P (2009) Functional changes in CSF volume estimated using measurement of water T2 relaxation. *Magn Reson Med* 61(3):579–586
21. Duong TQ, Kim SG (2000) In vivo MR measurements of regional arterial and venous blood volume fractions in intact rat brain. *Magn Reson Med* 43(3):393–402
22. Duong TQ, Yacoub E, Adriany G, Hu X, Ugurbil K, Kim SG (2003) Microvascular BOLD contribution at 4 and 7 T in the human brain: gradient-echo and spin-echo fMRI with suppression of blood effects. *Magn Reson Med* 49(6):1019–1027
23. Kwong KK, McKinstry RC, Chien D, Rosen BR (1991) Is the biexponential signal decay in diffusion imaging due primarily to cerebrospinal fluid? In: Proceedings of the 9th annual meeting, Society for Magnetic Resonance Imaging. Chicago, p 201
24. Wetscherek A, Stieltjes B, Semmler W, Laun FB (2011) Investigation of the theoretical background of the IVIM model using flow compensated DWI. In: Proceedings of the 19th scientific meeting, International Society for Magnetic Resonance in Medicine, Montreal, p 2991
25. Cho GY, Kim S, Jensen JH, Storey P, Sodickson DK, Sigmund EE (2012) A versatile flow phantom for intravoxel incoherent motion MRI. *Magn Reson Med* 67(6):1710–1720
26. Le Bihan D, Turner R (1992) The capillary network: a link between IVIM and classical perfusion. *Magn Reson Med* 27(1):171–178
27. Kwong KK, McKinstry RC, Chien D, Crawley AP, Pearlman JD, Rosen BR (1991) CSF-suppressed quantitative single-shot diffusion imaging. *Magn Reson Med* 21(1):157–163
28. Mori S (2006) Introduction to diffusion tensor imaging. Elsevier, Boston, Amsterdam
29. Falconer JC, Narayana PA (1997) Cerebrospinal fluid-suppressed high-resolution diffusion imaging of human brain. *Magn Reson Med* 37(1):119–123